Journal of Materials Chemistry

Cite this: J. Mater. Chem., 2012, 22, 4652

www.rsc.org/materials

PAPER

Novel nano-materials, RGD-tetrapeptide-modified 17β-amino-11α-hydroxyandrost-1,4-diene-3-one: synthesis, self-assembly based nano-images and *in vivo* anti-osteoporosis evaluation†

Yuji Wang, Jianhui Wu, Guifeng Kang, Ming Zhao,* Lin Gui, Ning Li, Li Peng, Xiaoyi Zhang, Li Li and Shiqi Peng*

Received 16th August 2011, Accepted 13th December 2011
DOI: 10.1039/c2jm13983a

To find novel nano-materials with anti-osteoporosis activity and without side effects three novel anti-osteoporosis active amphiphiles, 17β-(RGD-AA-amido)-11α-hydroxyandrost-1,4-diene-3-one (**5a**: AA = Ser, **5b**: AA = Val, **5c**: AA = Phe), were constructed by coupling the bone resorption inhibiting active RGD-peptides and anti-osteoporosis active 17β-amino-11α-hydroxyandrost-1,4-diene-3-one. In the solid state **5a**, **5b** and **5c** exist as dispersed globes of 300 nm–14 μm in diameter, dispersed eggs of 110 nm–19 μm in diameter and beads of 238 nm–22 μm in diameter, respectively. In ultrapure water 1.1 μM of **5a**, **5b** and **5c** form nano-globes of 33–400 nm, 16–278 nm and 54–187 nm in diameter, respectively. At an oral dose of 110 nmol kg^{-1} **5a–c** effectively inhibited mice from developing osteoporosis. In contrast to estradiol, **5a–c** did not induce mice to develop endometrial hyperplasia and thrombus.

1. Introduction

Self-organization or self-assembly is of practical importance in the formation of various ordered nanostructures in solution, in the bulk state, and on a solid surface, such as spherical, lamellar, honeycomb structures, and so on.[1] The advent of nano-materials opens a door to self-assembly.[2] Consequently, numerous self-assembling molecules, such as highly fluorinated amphiphilic molecules,[3] amphiphilic triblock copolymers with polyrotaxane as a central block,[4] amphiphilic dodecyl ester derivatives from aromatic amino acids,[5] dendritic molecules,[6] the shape anisotropy of non-spherical colloidal building blocks,[7] alkylated polycyclic aromatic hydrocarbons,[8] porphyrins, graphenes and fullerenes,[9] were designed. Of the self-assembling molecules, peptides have been considered a kind of special substance,[10–17] due to their ability to form nano-structures and to possess excellent bioactivity.[18]

It is commonly accepted that bone formation and bone resorption depend on the activity of osteoblasts and osteoclasts, respectively. In osteoporosis therapy estrogen has been administered because it is able to increase the activity of osteoblasts and decrease the activity of osteoclasts.[19–21] By blocking the adhesiveness of osteoclasts onto the surface of the bone RGD-tetrapeptides can inhibit bone resorption.[22] The conjugates of RGD-tetrapeptides and estrogen were explored and proved to be able to improve the anti-osteoporosis potency and reduce endometrial hyperplasia of estrogen therapy, but the thrombosis risk of estrogen therapy was not investigated.[23] In contrast to estrogen, 17β-amino-11α-hydroxyandrost-1,4-diene-3-one, a novel anti-osteoporosis androgene, possesses higher efficacy, does not induce endometrial hyperplasia and thrombosis risk.[24] To find novel amphiphilic molecules with anti-osteoporosis activity and without side effects, this paper introduced RGD-tetrapeptides into 17β-amino-11α-hydroxyandrost-1,4-diene-3-one to form three 17β-(Arg-Gly-Asp-AA-amido)-11α-hydroxyandrost-1,4-diene-3-one (**5a–c**, AA = Ser, Val or Phe), evaluated their *in vivo* anti-osteoporosis activities, examined their endometrial hyperplasia and thrombosis risks, measured their scanning electron microscopy (SEM) and transmission electron microscope (TEM) images and discussed the relationship between their anti-osteoporosis action, side effects and nanostructure.

2. Experimental

2.1. General

The protected amino acids with L-configuration were purchased from Sigma Chemical Co. All coupling and deprotective reactions were carried out under anhydrous conditions. Chromatography was performed on Qingdao silica gel H. The purities of the intermediates were measured with TLC (Merck silica gel plates of type 60 F_{254}, 0.25 mm layer thickness) and were more than 95%. The purities of the products were measured with HPLC (Waters, C_{18} column 4.6 × 150 mm) and were more than 97%. All reagents were of commercial quality and were used as

College of Pharmaceutical Sciences, Capital Medical University, Beijing, 100069, P. R. China. E-mail: maozhao@126.com; Tel: +86-10-8391-1535; sqpeng@bjmu.edu.cn; +86-10-8391-1528

† Electronic Supplementary Information (ESI) available. See DOI:10.1039/c2jm13983a

received. Solvents were dried and purified using standard techniques when it was necessary. Reactions were monitored by thin layer chromatography, on glass plates coated with silica gel with a fluorescent indicator. Melting points were measured on a XT5 hot stage microscope (Beijing keyi electro-optic factory) and were uncorrected. Infrared spectra were recorded on a spectrophotometer (Perkin-Elmer 983 instrument), and the solid compounds were compressed into KBr pellets. ^{1}H (500 M Hz) and ^{13}C (125 M Hz) NMR spectra were recorded on a Bruker Avance II 500 MHz spectrometer by use of DMSO-d_6 or $CDCl_3$ as the solvent and tetramethylsilane as the internal standard. ESI/MS was determined on a ZQ2000 (Waters, US). The content of calcium was measured on a Varian SpectrAA 220 instrument. Bone trabecular density was measured on a STRATEC XCT Research SA+ instrument.

2.2. Synthesis of 5a–c

As indicated in Scheme 1, *via* a five-step-procedure **5a–c** were synthesized. The preparations and the data of intermediates **1**, **2a–c**, **3a–c** and **4a–c** are given in item 8 of ESI.†

2.2.1. Synthesis of 17β-(Arg-Gly-Asp-Ser-amido)-11α-hydroxyandrost-1,4-diene-3-one (5a). A mixture of 400 mg (0.35 mmol) of **4a**, 1.5 ml of dimethyl sulfide, 1.5 ml of phenyl methyl ether and 3 ml of CF_3CO_2H/CF_3SO_3H (4 : 1) was stirred at 0 °C for 1.5 h. Upon removal of the excess CF_3CO_2H/CF_3SO_3H the residue was triturated with ether and then purified on Sephadex-G10 and HPLC to provide 190 mg (71%) of the title compound as a light yellow powder. Mp 114–116 °C, $[\alpha]_D^{20} = 4.0$ ($c = 0.13$, MeOH), ESI-MS (*m*/*z*) 717 $[M + H]^+$. ^{1}H NMR (500 MHz, DMSO-d_6) δ (ppm) = 10.64 (w, 1 H), 8.20 (s, 1 H), 8.15 (s, 2 H), 7.90 (s,1 H), 6.34 (dd, $J = 10.0$ Hz, 3.0 Hz, 1 H), 6.28 (d, $J = 3.0$ Hz,1 H), 6.10 (d, $J = 3.2$ Hz, 1 H), 4.99 (m, 1 H), 4.78 (m, 1 H), 4.10 (s, 2 H), 3.69 (t, $J = 9.5$ Hz, 1 H), 3.55 (m, 1 H), 3.16 (m, 1 H), 2.77 (d, $J = 11.0$ Hz, 2 H), 2.66 (t, $J = 11.2$ Hz, 2 H), 2.52 (b, 2 H), 2.44 (b, 1 H), 1.45–1.95 (m, 22 H), 1.96 (t, $J = 13.1$ Hz, 2 H), 1.46 (s, 3 H), 1.16 (s, 3 H). ^{13}C NMR (125 MHz, DMSO-d_6) δ (ppm) = 187.0, 180.0, 175.2, 170.2, 169.2, 166.0, 144.3, 136.5, 135.7, 123.5, 64.8, 61.2, 60.0, 56.7, 55.2, 50.1, 47.6, 43.0, 42.1, 38.4, 38.0, 37.2, 35.2, 31.7, 27.2, 25.8, 24.9, 19.2, 17,2, 14.9. Anal. Calcd. for $C_{34}H_{52}N_8O_9$: C, 56.97; H, 7.31; N, 15.63. Found: C, 57.18; H, 7.15; N, 15.85.

2.2.2. Synthesis of 17β-(Arg-Gly-Asp-Val-amido)-11α-hydroxyandrost-1,4-diene-3-one (5b). Using the procedure of preparing **5a** from 350 mg (0.33 mmol) of **4b** 170 mg (72%) of the title compound was obtained as a colorless powder. Mp 108–109 °C, $[\alpha]_D^{20} = 10.0$ ($c = 0.13$, MeOH), ESI-MS (*m*/*z*) 729 $[M + H]^+$. ^{1}H NMR (500 MHz, DMSO-d_6) δ (ppm) = 10.62 (w, 1 H), 8.24 (s, 1 H), 8.12 (s, 2 H), 7.91 (s, 1 H), 7.80 (s, 1 H), 6.35 (dd, $J = 11.0$ Hz, 3.0 Hz, 1 H), 6.27 (d, $J = 3.0$ Hz,1 H), 6.10 (d, $J = 3.0$ Hz, 1 H), 4.99 (m, 1 H), 4.78 (m, 1 H), 4.10 (s, 2 H), 3.69 (t, $J = 9.5$ Hz, 1 H), 3.55 (m, 1 H), 3.16 (m, 1 H), 2.77 (d, $J = 11.1$ Hz, 2 H), 2.68 (m, 2 H), 2.66 (t, $J = 11.2$ Hz, 2 H), 2.52 (b, 2 H), 2.50 (b, 1 H), 1.45–1.95 (m, 17 H), 1.96 (t, $J = 12.0$ Hz, 2 H), 1.46 (s, 3 H), 1.16 (s, 3 H), 1.03 (d, $J = 10.1$ Hz, 6 H). ^{13}C NMR (125 MHz, DMSO-d_6) δ (ppm) = 187.1, 182.1, 175.5, 171.5, 165.3, 144.1, 138.5, 136.0, 132.4, 128.6, 67.8, 62.2, 60.0, 56.8, 56.1, 50.6, 43.5, 43.0, 38.3, 38.0, 37.2, 35.2, 31.7, 29.0, 27.2, 25.8, 24.9, 19.2, 17,2, 16.2, 14.9. Anal. Calcd. for $C_{36}H_{56}N_8O_8$: C, 59.32; H, 7.74; N, 15.37. Found: C, 59.50; H, 7.60; N, 15.14.

2.2.3. Synthesis of 17β-(Arg-Gly-Asp-Phe-amido)-11α-hydroxyandrost-1,4-diene-3-one (5c). Using the procedure of preparing **5a** from 460 mg (0.41 mmol) of **4c** 240 mg (75%) of the title compound was obtained as a colorless powder. Mp 112–113 °C, $[\alpha]_D^{20} = 14.0$ ($c = 0.12$, MeOH), ESI-MS (*m*/*z*) 777 $[M + H]^+$. ^{1}H NMR (500 MHz, DMSO-d_6) δ (ppm) = 10.77 (w, 1 H), 8.21 (s, 1 H), 8.10 (s, 1 H), 7.93 (s, 1 H), 7.85 (s, 1 H), 7.06–7.22 (m, 5 H), 6.36 (dd, $J = 11.1$ Hz, 3.0 Hz, 1 H), 6.28 (d, $J = 3.0$ Hz, 1 H), 6.10 (d, $J = 3.1$ Hz, 1 H), 4.94 (m, 1 H), 4.74 (m, 1 H), 4.12 (s, 2 H), 3.54 (t, $J = 9.5$ Hz, 1 H), 3.52 (m, 1 H), 3.16 (m, 1 H), 2.77 (d, $J = 11.2$ Hz, 2 H), 2.66 (m, 2 H), 2.64 (t, $J = 11.2$ Hz. 2 H),

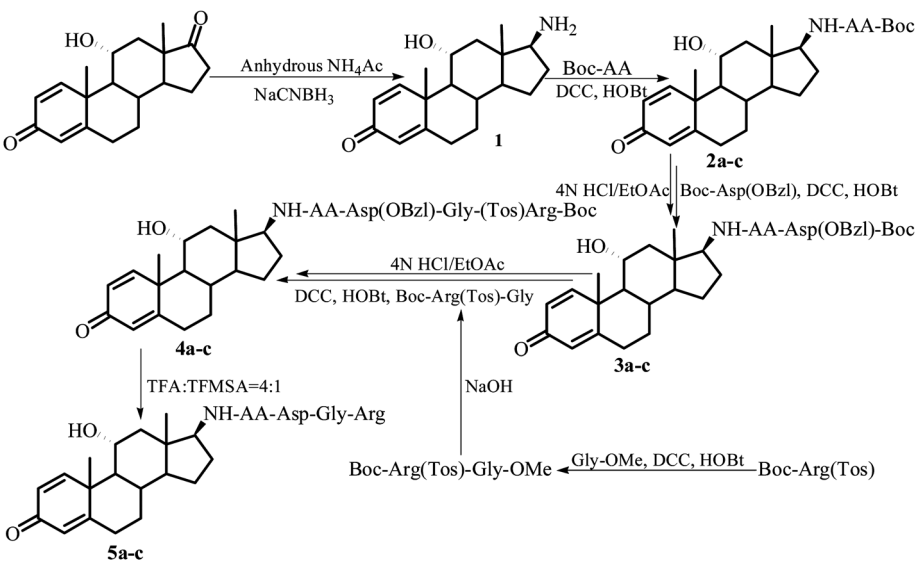

Scheme 1 Synthesis route to 17β-(Arg-Gly-Asp-Ser/Val/Phe-amido)-11α-hydroxyandrost-1,4-diene-3-ones. In **2a–4a**: AA = Ser(Bzl); in **5a**, AA = Ser; in **2b–5b**: AA = Val; in **2c–5c**: AA = Phe.

2.52 (b, 2 H), 2.30 (b, 1 H), 1.45–1.96 (m, 19 H), 1.96 (t, $J = 13.0$ Hz, 2 H), 1.46 (s, 3 H), 1.16 (s, 3 H). ^{13}C NMR (125 MHz, DMSO-d_6) δ (ppm) = 187.2, 178.0, 175.2, 171.2, 166.6, 144.3, 140.2, 136.5, 135.7, 132.5, 128.2, 125.8, 123.4, 62.2, 60.0, 56.6, 54.2, 50.2, 43.2, 43.0, 39.2, 38.0, 37.4, 35.2, 30.3, 29.5, 28.1, 25.5, 20.0, 18.4, 17,1, 15.7. Anal. Calcd. for $C_{40}H_{56}N_8O_8$: C, 61.84; H, 7.27; N, 14.42. Found: C, 61.62; H, 7.11; N, 14.66.

2.3. Evaluation of the *in vivo* anti-osteoporosis and side effects of 5a–c

2.3.1. Animals and administration. The assessments described herein were performed based on a protocol reviewed and approved by the ethics committee of Capital Medical University. The committee assured that the welfare of the animals was maintained in accordance to the requirements of the animal welfare act and according to the guide for care and use of laboratory animals. ICR mice (weighing 20.7 ± 2.1 g, purchased from Animal Center of Peking University) were housed under temperature and humidity controlled conditions at a 12 h light and 12 h dark (6 pm to 6 am) cycle for one day before being used. Each of them in drug receiving groups was administered special food (containing 0.1% of calcium and 0.4% of phosphorus) and distilled water, while each of them in blank control was administered normal food (containing 1.76% of calcium and 1.01% of phosphorus) and running water. Each mouse in the prednisone control group was injected with 6.3 mg kg^{-1} of prednisone, intramuscularly, twice a week and orally administered 0.2 mL of distilled water once a day. Each mouse in the treated group was injected with 6.3 mg kg^{-1} of prednisone, intramuscularly, twice a week and orally administered 110 nmol kg^{-1} of **5a–c** in 0.2 of distilled water once a day. All mice were treated in the corresponding way for 4 weeks. On the next day of the last administration the mice were weighed, blood was drawn *via* an eye orbit, the mice were then sacrificed with pentobarbital sodium (40.0 mg kg^{-1}, i.p.) anesthesia, and immediately dissected to obtain the femurs and organs.

2.3.2. Testing the total and trabecula vBMD of the femurs of 5a–c treated mice. Secondary osteoporosis is common in patients treated with glucocorticoids and in prostate cancer patients receiving androgen deprivation therapy (ADT) in particular.[25–28] Chronic exposure to pharmacological doses of glucocorticoids, such as prednisone, causes multiple deleterious effects on osteopenia, osteoporosis and bone fracture in particular.[29–31] To evaluate the efficacy of **5a–c** preventing osteoporosis in female patients treated with glucocorticoids and male patients receiving ADT,[8–10] total volumetric bone mineral density (vBMD) and trabecula vBMD tests were performed.

Computed tomography (CT) allows the measurement of 3D bone geometry, and could provide measurements of size-independent vBMD. Peripheral quantitative CT (pQCT) allows the quantitative measurement of 3D bone geometry, and could provide quantitative measurements of size-independent vBMD. In the present pQCT tests normal saline (NS) only was used as the background control and NS plus prednisone was used as the blank control to measure the total vBMD and trabecular vBMD of the femurs of **5a–c** plus prednisone treated mice.

2.3.3. Testing the bone weight and mineral content of 5a–c treated mice. After execution the left femurs of the mice were immediately collected, on complete removal of the muscle their lengths were measured, and then they were immersed in a 2 : 1 solution of chloroform and methanol twice (each 3 h). After being defatted the left femurs were heated at 120 °C for 6 h, cooled and weighed to record their dry weight. The femurs were calcined in a furnace at 800 °C for 8 h, cooled, weighed to record the ash weight, and the rate of the ash weight to dry femur weight (the mineral content of the femur) was calculated. The ashes of the left femurs were dissolved in 0.5 mL of hydrochloric acid (6 N) and diluted to 5.00 mL with ultrapure water, from which 0.05 mL of the solution was drawn and diluted to 1.00 mL with ultrapure water before use. The calcium content of the aqueous solution was measured with the method of *o*-methylphenolphthalein complexing ketone. The phosphorus content of the aqueous solution was measured with the method of molybdenum blue.

2.3.4. Testing the bleeding cease time of 5a–c treated mice. After the 4 week treatment with estradiol or **5a–c** the mice in anti-osteoporosis assays were weighed to record the body weights. Thirty and ninety min after the last administration, the mice were subjected to an *in vivo* tail bleeding time assay by use of a standard procedure. Briefly, the mouse was placed in a tube holder with its tail protruding, and a 2 mm cut was made on the tail. Flowing blood until it stopped was gently wiped away with a filter paper every 30 s, yielding the bleeding time.

2.3.5. Testing the uterine weight of 5a–c treated mice. After the 4 week treatment with estradiol or **5a–c** the mice in anti-osteoporosis assays were sacrificed with pentobarbital sodium (40.0 mg kg^{-1}, i.p.) anesthesia and immediately dissected to obtain the uterus to record their weights.

2.4. Identification of the nano-characterization of 5a–c

2.4.1. Measuring the SEM images of 5a–c in solid state. The shape and size of the nano-species of the lyophilizing powders of 1.1 μM solutions of **5a–c** in ultrapure water were measured on a SEM (JEM-1230, JEOL, Tokyo, Japan) at 50 kV. The lyophilizing powders were attached on to a copper plate *via* double-side tape (Euromedex, France). The specimens were coated with 20 nm gold–palladium using a JEOL JFC-1600 AUTO FINE COATER. The coater was operated at 15 kV, 30 mA, 200 mTorr (argon) for 60 s. The shape and size distribution of the nano-particles were measured from counting over 100 particles in randomly selected regions on the SEM alloy. All the measurements in triplicate grids were performed. The images were recorded on an imaging plate (Gatan Bioscan Camera Model1792) with 20 eV energy windows at 100–10 000×, and were digitally enlarged.

2.4.2. Measuring the TEM images of 5a–c in water. The shape and size of the nano-species of **5a–c** were measured on a TEM (JSM-6360 LV, JEOL, Tokyo, Japan). The solution (1.1 μM) of **5a–c** in ultrapure water was dripped onto a formvar-coated copper grid and then a drop of anhydrous ethanol was added to promote the removal of water. At first the grid was

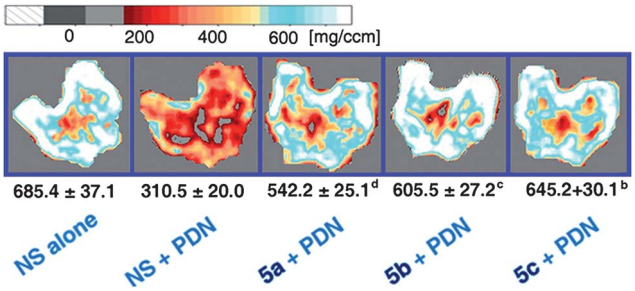

Fig. 1 Total vBMD and images of pQCT scanning at a distance from the proximal femur growth palate corresponding to <6% of the total length of the femur of the treated mice.

allowed to thoroughly dry in air and then heated at 35 °C for 24 h. The sample was viewed under the TEM. The shape and size of the nano-species on the TEM copper grid were obtained from counting over 100 species in randomly selected regions. All determinations were carried out in triplicate grids. TEM was operated at 80 kV electron beam accelerating voltage. The images were recorded on an imaging plate (Gatan Bioscan Camera Model 1792) with 20 eV energy windows at 6000–400 000×, and were digitally enlarged.

2.4.3. Measuring the nano-size of 5a–c in NS. The size of the nano-particles of **5a–c** in NS was measured on a Malvern's Zeta Sizer (Nano-ZS90) with DTS (Nano) Program. The concentration of the solution of **5a–c** in NS was 1.1 μM, the testing temperature was 25 °C, the time interval was 30 s, the mean size and half-peak width of ten times were recorded.

2.4.4. Measuring the zeta-potential of 5a–c in NS. The zeta-potential of the surface of nano-particles of **5a–c** in NS was measured on a ZetaPlus Potential Analyzer (ZetaPlus S/N 21394, Brookhaven Instruments Coorporation) with BIC Zeta Potential Analyzer. The concentration of the solution of **5a–c** in NS was 1.1 μM and the testing temperature was 25 °C. The zeta potential

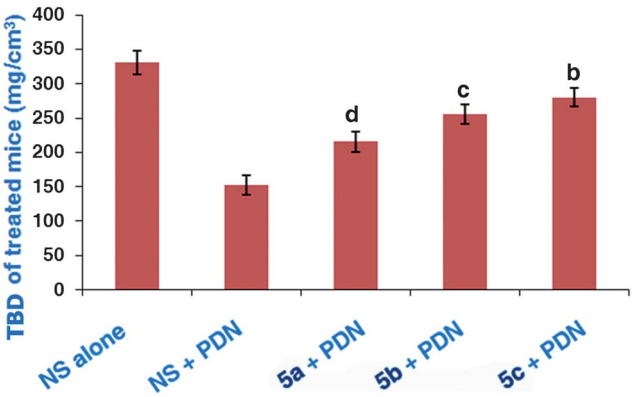

Fig. 2 Trabecular vBMD of the femurs of the treated mice at a distance from the proximal femur growth palate corresponding to <6% of the total length of the femurs of the treated mice. a) Trabecular vBMD is represented with mean ± SD mg cm^{-3}, $n = 12$, PDN = prednisone, dose of **5a–c** = 110 nmol kg^{-1}. b) Compared to NS + PDN, **5a** + PDN and **5b** + PDN $p < 0.01$. c) Compared to NS + PDN and **5a** + PDN $p < 0.01$. d) Compared to NS + PDN $p < 0.01$.

measurement was repeated for 3 runs per sample, and the data were calculated automatically using the software from the electrophoretic mobility based on Smoluchowski's formula.

3. Results and discussion

3.1. Chemical synthesis of 5a–c

As indicated in Scheme 1, *via* a five-step-procedure **5a–c** were prepared. In brief, the reduction of 11α-hydroxyandrost-1,4-diene-3,17-dione provided 17β-amino-11α-hydroxyandrost-1,4-diene-3,17-dione (**1**, 90% yield), the coupling of **1** and Boc-Ser(Bzl), Boc-Val or Boc-Phe provided 17β-[Boc-Ser(Bzl)-amido]- or 17β-[Boc-Val-amido]- or 17β-[Boc-Phe-amido]-11α-hydroxyandrost-1,4-diene-3-ones (**2a–c**, 82–84% yields). After removing Boc, **2a–c** were coupled with Boc-Asp to provide 17β-(Boc-Asp-Ser(Bzl)-amido)- or 17β-(Boc-Asp-Val-amido)- or 17β-(Boc-Asp-Phe-amido)-11α-hydroxyandrost-1,4-diene-3-one (**3a–c**, 88–94% yields). After removing Boc, **3a–c** were coupled with Boc-Arg(Tos)-Gly to provide 17β-(Boc-Arg(Tos)-Gly-Asp-Ser(Bzl)-amido)- or 17β-(Boc-Arg(Tos)-Gly-Asp-Val-amido)- or 17β-(Boc-Arg(Tos)-Gly-Asp-Phe-amido)-11α-hydroxyandrost-1,4-diene-3-one (**3a–c**, 88–94% yields). In the presence of CF_3CO_2H/CF_3SO_3H all protective groups were removed and **5a–c** were obtained in 72% to 75% yields. Besides, Boc-Arg(Tos)-Gly was prepared by using the solution method and the yield was

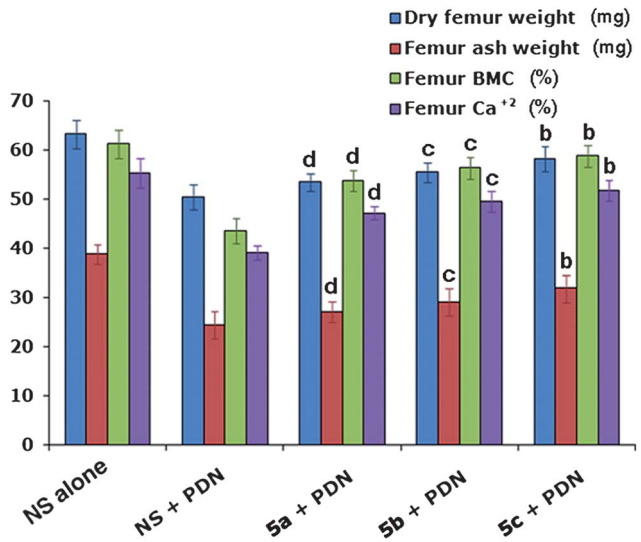

Fig. 3 Dry weights, ash weights, Ca^{2+} and BMC of the femurs of **5a–c** treated mice. a) Weights of dry femur and femur ash are represented with mean ± SD mg, femur Ca^{2+} and BMC is represented with mean ± SD %, $n = 12$, PDN = prednisone, dose of **5a–c** = 110 nmol kg^{-1}. **For dry femur weight:** b) compared to NS + PDN and **5a** + PDN $p < 0.01$, to **5b** + PDN $p < 0.05$; c) compared to NS + PDN $p < 0.01$, to **5a** + PDN $p < 0.05$; d) compared to NS + PDN $p < 0.01$. **For femur ash weight:** b) compared to NS + PDN, **5b** + PDN and **5a** + PDN $p < 0.01$; c) compared to NS + PDN $p < 0.01$, to **5a** + PDN $p < 0.05$; d) compared to NS + PDN $p < 0.01$. **For femur BMC:** b) compared to NS + PDN and **5c** + PDN $p < 0.01$, to **5b** + PDN $p < 0.05$; c) compared to NS + PDN $p < 0.01$, to **5a** + PDN $p < 0.05$; d) compared to NS + PDN $p < 0.01$. **For femur Ca^{2+} :** b) compared to NS + PDN and **5a** + PDN $p < 0.01$, to **5b** + PDN $p < 0.05$; c) compared to NS + PDN $p < 0.01$, to **5a** + PDN $p < 0.05$; d) compared to NS + PDN $p < 0.01$.

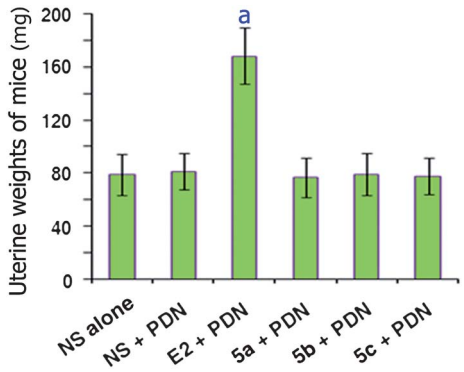

Fig. 4 Uterine weights of **5a–c** treated mice. Uterine weight is represented by mean ± SD mg, $n = 12$, PDN = prednisone, E2 = estradiol, dose of E2 and **5a–c** = 110 nmol kg^{-1}. a) Compared to NS alone $p < 0.01$.

at the same level as that reported previously.[23,24] This five-step-procedure is suitable for preparing **5a–c**.

3.2. Total and trabecula vBMD of the femurs of 5a–c treated mice

CT measured 3D bone geometry and the size-independent vBMD, as well as pQCT quantitatively measured 3D bone geometry and size-independent vBMD were used to represent the anti-osteoporosis efficacy of **5a–c** and are shown in Fig. 1 and 2.

Fig. 1 indicates that the total vBMD of the femurs of NS plus prednisone treated mice is significantly lower than that of the femurs of NS alone treated mice. This means that prednisone effectively induces the mice to decrease the total vBMD. The total vBMDs of the femurs of **5a–c** plus prednisone treated mice are significantly higher than those of the femurs of NS plus prednisone treated mice. This means that **5a–c** effectively inhibit prednisone treated mice to decrease the total vBMD. Besides, the total vBMD of the femurs of **5a** plus prednisone treated mice is significantly lower than those of the femurs of **5b** plus prednisone treated mice, while the total vBMD of the femurs of **5b** plus prednisone treated mice are significantly lower than those of the femurs of **5c** plus prednisone treated mice. This means that the activity order of **5a–c** inhibiting prednisone treated mice to develop osteoporosis is **5c** > **5b** > **5a**.

Fig. 2 indicates that the trabecular vBMD of the femurs of NS plus prednisone treated mice is significantly lower than that of the femurs of NS alone treated mice. This means that prednisone effectively induces the mice to decrease trabecular vBMD. The total trabecular vBMDs of the femurs of **5a–c** plus prednisone treated mice are significantly higher than those of the femurs of NS plus prednisone treated mice. This means that **5a–c** effectively inhibit prednisone treated mice to decrease trabecular vBMD. Besides, the trabecular vBMD of the femurs of **5a** plus prednisone treated mice is significantly lower than that of the femurs of **5b** plus prednisone treated mice, while the trabecular vBMD of the femurs of **5b** plus prednisone treated mice are significantly lower than that of the femurs of **5c** plus prednisone treated mice. This again means that the activity order of **5a–c** inhibiting prednisone treated mice to develop osteoporosis is **5c** > **5b** > **5a**.

3.3. Dry weights, ash weights, Ca^{2+} and BMC of the femurs of 5a–c treated mice

Physical and chemical studies were generally used in the *in vivo* anti-osteoporosis assay. In the present tests of the dry weights, ash weights, Ca^{2+} and bone mineral content (BMC) of the femurs of **5a–c** treated mice NS alone was used as the background control, NS plus prednisone was used as the blank control and the data are shown in Fig. 3.

Fig. 3 indicates that the dry weight of the femur of NS plus prednisone treated mice is significantly lower than that of the femur of NS alone treated mice. This means that prednisone effectively induces the mice to lose the femur. The dry weights of the femur of **5a–c** plus prednisone treated mice are significantly higher than those of the femur of NS plus prednisone treated mice. This means that **5a–c** effectively inhibit prednisone treated mice to lose femur. Similar effects of **5a–c** on femur ash weights, femur Ca^{+2} and femur BMC of the treated mice were also observed from Fig. 3. Besides, the activity order of **5a–c** inhibiting prednisone treated mice to lose femur's dry weights, femur's ash weights, femur's Ca^{2+} and femur's BMC is also **5c** > **5b** > **5a**.

3.4. Side effects of 5a–c *in vivo*

Endometrial hyperplasia and the thrombosis risk are common side effects in estrogen therapy. The endometrial hyperplasia risk of **5a–c** therapy is represented with the uterine weights of the treated mice and the data are shown in Fig. 4. The thrombosis risk of **5a–c** therapy is represented with the tail bleeding time of the treated mice and the data are shown in Fig. 5.

Fig. 4 indicates that the uterine weights of the mice receiving estradiol plus prednisone are significantly higher than those of the mice receiving NS alone. This means that estradiol therapy induces the mice to develop endometrial hyperplasia. In contrast to estradiol, the uterine weights of the mice receiving **5a–c** plus prednisone are equal to those of the mice receiving NS alone. This means that **5a–c** have no endometrial hyperplasia risk.

Fig. 5 indicates that 30 min and 90 min after of the last oral administration the tail bleeding times of the mice receiving estradiol plus predsone are significantly shorter than those of the mice receiving NS plus predsone. This means that estradiol therapy induces thrombosis risk. However 30 min and 90 min after of the last oral administration the tail bleeding times of the

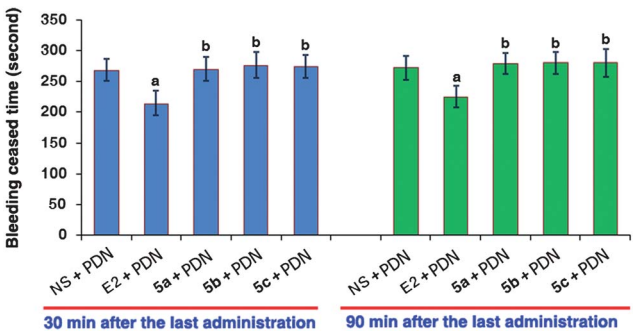

Fig. 5 Effect of **5a–c** on the tail bleeding time of the treated mice. Tail bleeding time is represented by mean ± SD s, $n = 12$, PDN = prednisone, E2 = estradiol. a) Compared to NS + PDN, $p < 0.01$; b) compared to NS + PDN, $p > 0.05$.

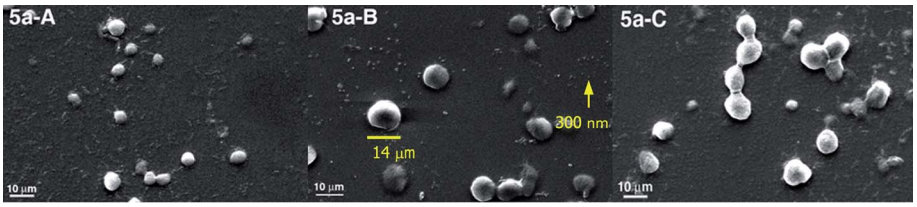

Fig. 6 SEM images of **5a** in solid state. Dispersing globes of 300 nm–14 μm in diameter (**5a**–A and **5a**–B), and fusion globes (**5a**–C).

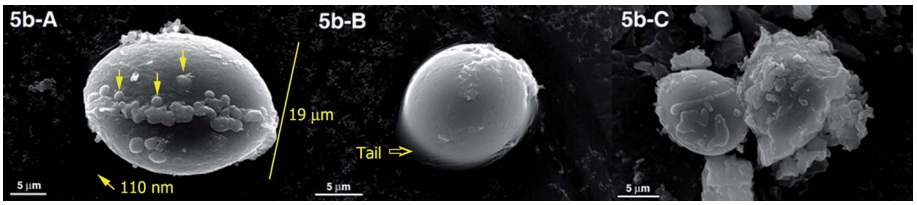

Fig. 7 SEM images of **5b** in solid state. Dispersing eggs of 110 nm–19 μm in diameter, a number of small eggs are on the faces of the four bigger eggs (**5b**–A, **5b**–B and **5b**–C), one egg remains with its tail incomplete, as well (**5b**–C).

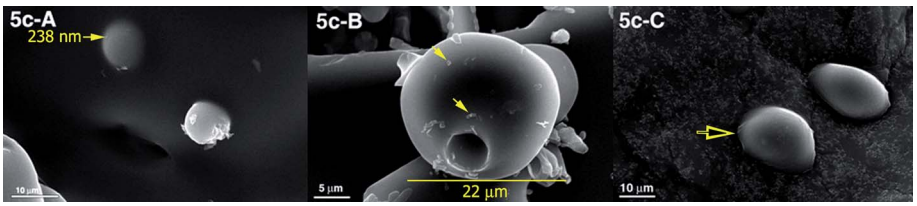

Fig. 8 SEM images of **5c** in solid state. Beads of 238 nm–22 μm in diameter, and some small beads are on the faces of the bigger beads (**5c**–A and **5c**–B), one side of a bead remains incomplete (**5c**–B and **5c**–C).

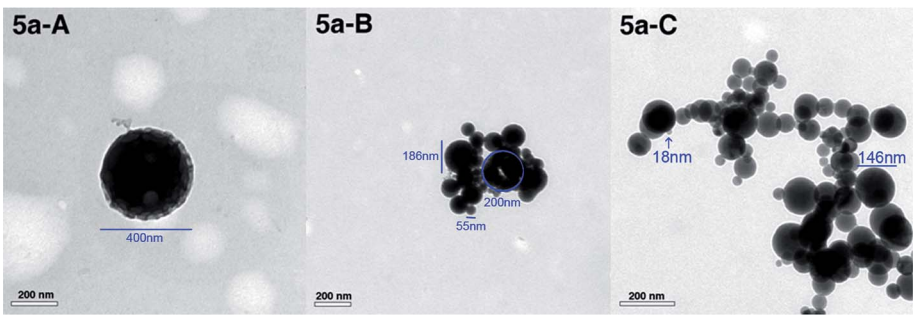

Fig. 9 TEM images of 1.1 μM of **5a** in ultrapure water. The nano-globe of 400 nm in diameter consists of numerous smaller globes (**5a**–A), the dispersing globes of 55–200 nm in diameter and some fusion globes (**5a**–B), as well as the dispersing globes of 18–146 nm in diameter (**5a**–C).

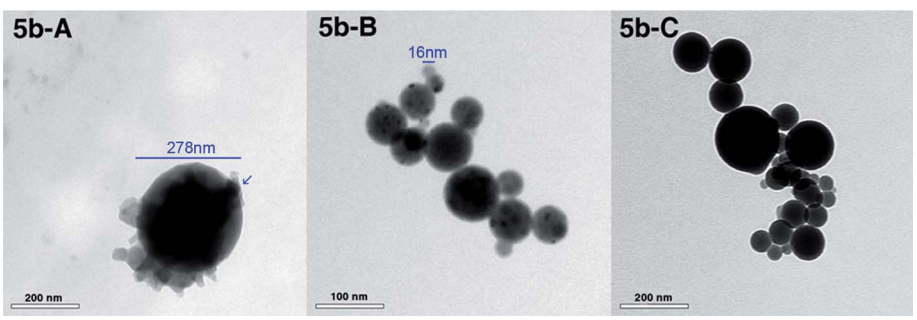

Fig. 10 TEM images of 1.1 μM of **5b** in ultrapure water. The smaller globes, blocks and awls are on the face of the larger globe in a fusion manner (**5b**–A), most of the nano-globes exist as separate objects, but four are fusion globes (**5b**–B) and similarly most of the nano-globes exist as separate objects, some are fusion globes (**5b**–C).

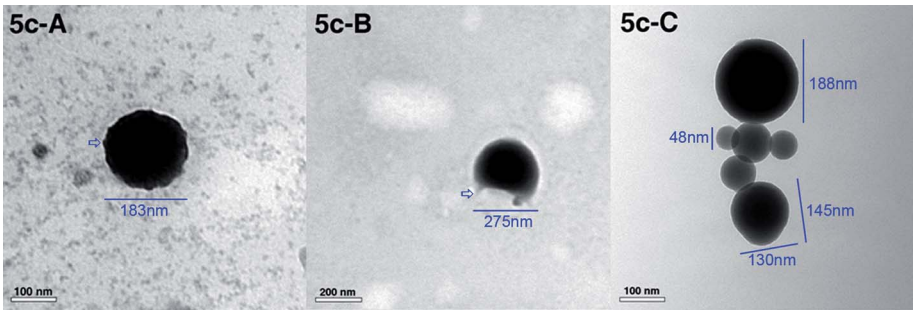

Fig. 11 TEM images of 1.1 μM of **5c** in ultrapure water. Numerous nano-particles and their aggregators spread around the nano-globe of 183 nm in diameter and a number of nano-particles are on its face in a fusion manner (**5c**–A), a hemisphere of 275 nm in diameter and some smaller globes adhere on its incomplete face (**5c**–B), five globes of 48–188 nm in diameter and one fusion globe of 130 × 145 nm (**5c**–C).

mice receiving **5a–c** plus predsone are equal to those of the mice receiving NS plus predsone. This means that **5a–c** therapy has no thrombosis risk.

3.5. Comparing *in vivo* activities and side effects of 5a–c with estradiol

The *in vivo* anti-osteoporosis activities, the endometrial hyperplasia risk and the thrombosis risk of **5a–c** were also compared with those of estradiol and the data are shown in Fig. 2, 3, 4, 5 and 7 of ESI.† The figures indicate that at the dose of 110 nmol kg^{-1} the *in vivo* anti-osteoporosis activities of oral **5a–c** are significantly higher than that of estradiol. Besides, in contrast to estradiol, **5a–c** do not induce the mice to develop endometrial hyperplasia and thrombus.

3.6. Comparing *in vivo* activities of 5a–c with 17β-amino-11α-hydroxyandrost-1,4-diene-3-one

The *in vivo* anti-osteoporosis activities of **5a–c** were further compared with that of the unmodified 17β-amino-11α-hydroxyandrost-1,4-diene-3-one, and the data are shown in Fig. 2, 3 and 4 of ESI.† The figures indicate that at the dose of 110 nmol kg^{-1} the *in vivo* anti-osteoporosis activities of oral **5a–c** are significantly higher than that of 17β-amino-11α-hydroxyandrost-1,4-diene-3-one. This means that the introduction of RGD-tetrapeptides enhances the *in vivo* anti-osteoporosis activity. Due to RGD-tetrapeptides being able to block the adhesiveness of osteoclasts onto the surface of the bone and lead **5a–c** to form nano-structures the enhanced *in vivo* anti-osteoporosis activities should be attributed to both the blockage of the adhesiveness of osteoclasts onto the surface of the bone and the formation of the nano-structures.

3.7. Nano-images of 5a–c

SEM and TEM have been widely used for the investigation of the three-dimensional structure of hydrogels, cells entrapped in nanofiber matrices or the individual nanostructures of peptides. To visualize the size and morphology of **5a–c** in solid state and in solution their SEM images and TEM images were measured and are shown in Fig. 6 to 8 and Fig. 9 to 11, respectively.

The SEM images demonstrate that in the solid state these amphiphilic molecules (**5a–c**) are able to self-assemble and form nano-globes or similar nano-species including nano-eggs and nano-beads. The similar characterization was observed in the TEM images of **5a–c**. This implies that it is the common chemical structure of 17β-(Arg-Gly-Asp-AA-amido)-11α-hydroxyandrost-1,4-diene-3-ones that determines the similarity of the nano-image characterization of **5a–c** in the solid state and in aqueous solution. On the other hand, the moiety 17β-amino-11α-hydroxyandrost-1,4-diene-3-one determines the size of the nano-globes and the amino acid residue of the C-terminus of the RGD-tetrapeptide moiety determines the feature of the nano-globes.

3.8. Sizes and zeta-potential of the nano-particles of 5a–c

As seen in Fig. 12, the mean diameters of the particles of **5a–c** are in a range of 128–266 nm during the monitored 10 days. In the first 5 days the diameters decrease gradually and in the second 5 days they have a relatively stable value. The mean diameters less than 270 nm could be attributed to the hydrophobicity of the 17β-amino-11α-hydroxyandrost-1,4-diene-3,17-dione moiety of **5a–c**, which leads to stronger hydrophobic interaction and the formation of aggregators with closer packing density. On the other hand, the order of the mean diameters is **5a** > **5b** > **5c**.

The zeta-potentials of the nano-globes of **5a–c** are in a range of 73.6–126.0 mV during the monitored 10 days, and the order of the zeta-potentials is **5a** < **5b** < **5c** (Fig. 13). This order matches the order of the mean diameters, *i.e.*, **5a** > **5b** > **5c**. The lower diameters and the higher zeta-potentials imply that the formed

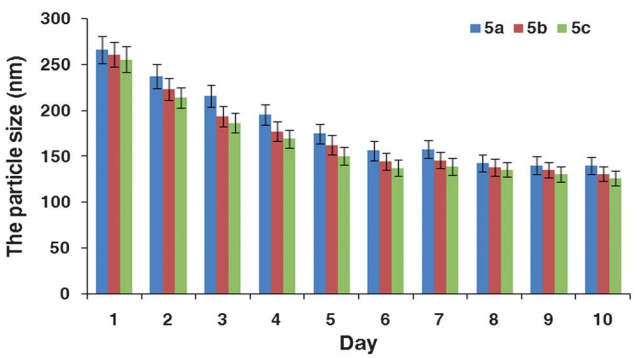

Fig. 12 Mean sizes of the particles of **5a–c** within 10 days.

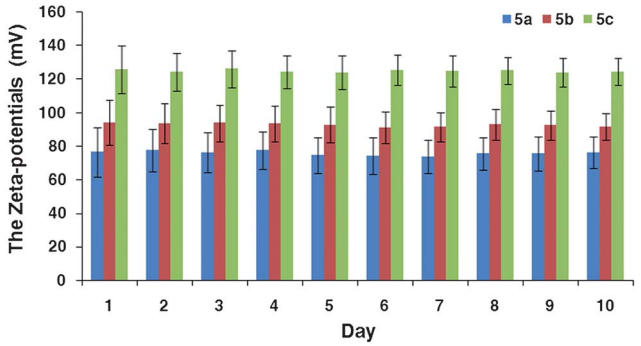

Fig. 13 Zeta-potentials of the particles of **5a–c** within 10 days.

nano-globes of **5a–c** in NS are stable nano-structures and benefit their *in vivo* transportation.

4. Conclusions

17β-(Arg-Gly-Asp-Ser-amido)-, 17β-(Arg-Gly-Asp-Val-amido)- and 17β-(Arg-Gly-Asp-Phe-amido)-11α-hydroxyandrost-1,4-diene-3-ones (**5a–c**) were disclosed as oral anti-osteoporosis agents for the first time. *In vivo* **5a–c** effectively inhibit prednisone treated mice to develop osteoporosis, and their efficacies are significantly higher than that of estradiol. In contrast to estradiol, **5a–c** neither induce the treated mice to develop endometrial hyperplasia, nor induce the treated mice to form a thrombus. In the solid state **5a–c** form nano-globes or similar nano-species *via* self-assembly. In solution **5a–c** form stable nano-globes or globe related nano-species *via* self-assembly. It is likely that the scaffold consisted of RGD-tetrapeptides and 17β-amino-11α-hydroxyandrost-1,4-diene-3-one determines the size of the nano-species, and the sequence of the RGD-tetrapeptide moiety determines the feature of the nano-species. Most of the nano-globes of the TEM images of **5a–c** have desirable diameters (<100 nm) and are able to escape the phagocytose of macrophages.[32]

Acknowledgements

This work was finished in Beijing Area Major Laboratory of Peptide and Small Molecular Drugs, supported by PHR (IHLB, KZ200910025-004 and KM200910025009), Innovation Platform Project of Education Committee of Beijing, Special Project (2011ZX09302-007-01), and Natural Scientific Foundation of China (81072522, 50801426).

References

1 H. Li, B. Song, L. Qin, Q. Liu, L. Wu and J. Shen, *J. Colloid Interface Sci.*, 2005, **290**, 557.
2 S. C. Glotzer, M. A. Horsch, C. R. Iacovella, Z. Zhang, E. R. Chan and X. Zhang, *Curr. Opin. Colloid Interface Sci.*, 2005, **10**, 287.
3 R. T. M. Jakobs, J. van Herrikhuyzen, J. C. Gielen, P. C. M. Christianen, S. C. J. Meskers and A. P. H. J. Schenning, *J. Mater. Chem.*, 2008, **18**, 3438.
4 X. Zhang, X. Zhu, F. Ke, L. Ye, E. Chen, A. Zhang and Z. Feng, *Polymer*, 2009, **50**, 4343.
5 R. Vijay, S. Angayarkanny and G. Baskar, *Colloids Surf., A*, 2008, **317**, 643.
6 E. Mehdipoor, M. Adeli, M. Bavadi, P. Sasanpour and B. Rashidian, *J. Mater. Chem.*, 2011, **21**, 15456.
7 S. Sacanna and D. J. Pine, *Curr. Opin. Colloid Interface Sci.*, 2011, **16**, 96.
8 V. Palermo, M. Palma, Ž. Tomović, M. D. Watson, K. Müllen and P. Samorì, *Synth. Met.*, 2004, **147**, 117.
9 S. Gadipelli, I. Calizo, J. Ford, G. Cheng, A. R. Hight Walker and T. Yildirim, *J. Mater. Chem.*, 2011, **21**, 16057.
10 L. S. Witus, J. R. Rocha, V. M. Yuwono, S. E. Paramonov, R. B. Weisman and J. D. Hartgerink, *J. Mater. Chem.*, 2007, **17**, 1909.
11 G. Palui, S. Ray and A. Banerjee, *J. Mater. Chem.*, 2009, **19**, 3457.
12 V. Castelletto and I. W. Hamley, *Biophys. Chem.*, 2009, **141**, 169.
13 H. G. Börner, *Prog. Polym. Sci.*, 2009, **34**, 811.
14 A. Carlsen and S. Lecommandoux, *Curr. Opin. Colloid Interface Sci.*, 2009, **14**, 329.
15 E. K. Johnson, D. J. Adams and P. J. Cameron, *J. Mater. Chem.*, 2011, **21**, 2024.
16 N. Wiradharma, Y. W. Tong and Y. Yang, *Biomaterials*, 2009, **30**, 3100.
17 V. Gribova, T. Crouzier and C. Picart, *J. Mater. Chem.*, 2011, **21**, 14354.
18 N. Li, G. Kang, L. Gui, M. Zhao, W. Wang, J. Zhang, Y. Yue and S. Peng, *Nanomed.: Nanotechnol., Biol. Med.*, 2011, **7**, 403.
19 Y. Lim and M. Lee, *J. Mater. Chem.*, 2008, **18**, 723.
20 K. J. Majeska, J. T. Ryaby and T. A. Einhorn, *J. Bone J. Surg., Am. Vol.*, 1994, **76**, 713.
21 X. Y. Zang, Y. B. Tan, Z. L. Pang, W. Z. Zhang and J. Zhao, *Chin. Med. J.*, 1994, **107**, 600.
22 M. A. Horton, M. L. Taylor, T. R. Arnett and M. H. Helfrich, *Exp. Cell Res.*, 1991, **195**, 368.
23 Y. Xiong, M. Zhao, C. Wang, H. Chang and S. Peng, *J. Med. Chem.*, 2007, **50**, 3340.
24 C. Li, S. Peng, M. Zhao, N. Li and F. Wu, Application No: CN200710090291.8.
25 A. Kelman, *Best Pract. Res. Clin. Rheumatol.*, 2005, **19**, 1021.
26 H. Liu, N. M. Paige, C. L. Goldzweig, E. Wong, A. Zhou, M. J. Suttorp, B. Munjas, E. Orwoll and P. Shekelle, *Ann. Intern. Med.*, 2008, **148**, 685.
27 R. W. Ross and E. J. Small, *J. Urol.*, 2002, **167**, 1952.
28 D. Cohen and J. D. Adachi, *J. Steroid Biochem. Mol. Biol.*, 2004, **88**, 337.
29 F. Manelli and A. Giustina, *Trends Endocrinol. Metab.*, 2000, **11**, 79.
30 S. M. H. Alibhai, S. Gogov and Z. Allibhai, *Crit. Rev. Oncol. Hematol.*, 2006, **60**, 201.
31 R. A. Adlera, *Maturitas*, 2011, **68**, 143.
32 Y. Fujita, M. Mie and E. Kobatake, *Biomaterials*, 2009, **30**, 3450.